

DOI: 10.1002/ ((please add manuscript number))

Article type: Communication

Solution-processed MoS₂/ organolead trihalide perovskite photodetectors

*Yan Wang, Raymond Fullon, Muharrem Acerce, Christopher E. Petoukhoff, Jieun Yang, Chenggan Chen, Songnan Du, Sin Ki Lai, Shu Ping Lau, Damien Voiry, Gautam Gupta, Aditya D. Mohite, Shengdong Zhang, Hang Zhou, * and Manish Chhowalla**

Y. Wang, R. Fullon, M. Acerce, C. E. Petoukhoff, Dr. J. Yang, Dr. D. Voiry, Prof. M. Chhowalla

Materials Science and Engineering, Rutgers University, 607 Taylor Road, Piscataway, New Jersey 08854, USA

Email: manish1@rci.rutgers.edu

Y. Wang, C. Chen, S. Du, Prof. S. Zhang, Prof. H. Zhou

Shenzhen Key Lab of Thin Film Transistor and Advanced Display, Peking University Shenzhen Graduate School, Peking University, Shenzhen 518055, China

Email: zhouh81@pkusz.edu.cn

S. K. Lai, Prof. S. P. Lau

Department of Applied Physics, The Hong Kong Polytechnic University, Hung Hom, Kowloon HKSAR, Hong Kong

Prof. G. Gupta, Prof. A. D. Mohite

MPA-11 Materials Synthesis and Integrated Devices, Los Alamos National Laboratory, Los Alamos, New Mexico 87545, USA

Keywords: MoS₂, perovskite, photodetector

Integration of heterogeneous materials provides opportunities for realizing new types of electronic and opto-electronic devices with increased performance. Two dimensional (2D) materials such as single or few layered transition metal dichalcogenides (TMDs) exhibit interesting optical and electronic properties that are of fundamental as well as technological interests.^[1] The integration of 2D materials with other low dimensional materials such as single walled carbon nanotubes^[2] or PbS quantum dots^[3] leads to substantial enhancement in the light absorption and quantum efficiency which in turn can substantially improve the responsivity of a photodetector.^[4] Incorporation of 3D or molecular absorption layers such as amorphous silicon^[5] and rhodamine 6G fluorescent dye^[6] can also modify light matter interactions in 2D

materials. Like 2D TMDs, organolead trihalide perovskites with formula of MAPbX_3 (MA = methylammonium CH_3NH_3 and X = halogen) possess interesting optical and electronic properties such as long free carrier diffusion lengths and high absorption, which results in excellent solar cell performance.^[7,8] The integration of lead halide perovskites with 2D TMDs and other layered materials, therefore, offers opportunities for studying unique charge transfer mechanisms and light matter interactions in devices such as photodetectors. To this end, perovskites have been integrated as absorption layers on graphene,^[9–11] reduced graphene oxide^[12] and MoS_2 ^[12] and WSe_2 ^[14] to improve photoresponsivity in photodetectors. A key challenge in integrated perovskite/2D materials photodetectors is to improve the photoresponsivity while maintaining a low dark state current. That is for a highly conducting 2D layer such as graphene, substantial current is present in the dark (or off) state and the relative enhancement in the photo (or on state) current is low and therefore the overall on/off ratio is impractical. Furthermore, most studies utilize 2D layers that are deposited by either chemical vapor deposition or mechanical exfoliation. Large area solution based deposition of high quality chemically exfoliated 2D materials could provide ease of fabrication and allows many integrated devices over large areas to be tested.

In this study, we have fabricated solution-processed heterostructures consisting of 2D MoS_2 and perovskite with device structure illustrated in **Figure 1a** for photodetection. Bulk MoS_2 powder was chemically exfoliated using the well-established lithium intercalation method into monolayer nanosheets that are soluble in water.^[15] We have reported the detailed characterization of 2D chemically exfoliated MoS_2 nanosheets elsewhere in several published reports.^[15–17] The nanosheets fabricated here were characterized with Raman and x-ray photoelectron spectroscopies (XPS) to obtain the concentration of the metallic and

semiconducting phases. Uniform deposition of MoS₂ nanosheets was carried out using vacuum filtration and transfer onto the target substrate.^[18] It is well known that 2D MoS₂ can exist in either the semiconducting trigonal prismatic (2H phase) or the metallic octahedral (1T phase) crystal structures.^[19] Chemical exfoliation of bulk MoS₂ using lithium intercalation leads to nanosheets that are primarily 1T phase and therefore electrically conducting.^[20] The 1T phase of MoS₂ is metastable and can be relaxed to the thermodynamically stable 2H-MoS₂ phase by annealing at 300 °C in vacuum or argon for 2 hours.^[15] The 1T phase concentration in the exfoliated nanosheets is ~ 70% at room temperature but decreases to 0% (or 100% 2H phase) after annealing at 300 °C.

The thickness of the solution processed thin films of MoS₂ nanosheets can be precisely controlled by vacuum filtration. We have systematically investigated the effect of the MoS₂ thickness and phase on the performance of the photodetectors. We fabricated devices using three thicknesses of 1T and 2H phase MoS₂ nanosheets while keeping the thickness of the perovskite film constant. The thicknesses of MoS₂ nanosheet films correspond to an electrically percolating but not fully continuous layer (~80% coverage of the channel surface), completely continuous channel film with full coverage, and thick multi-layered film. An optical microscopy image of the device with continuous MoS₂ film is shown in Figure 1b, the blue area is MoS₂ film deposited on silicon oxide and the pink rectangle is patterned gold electrodes. Optical images of different thicknesses of MoS₂ are given in the supplementary information (Figure S1). A corresponding atomic force microscope (AFM) image showing 2D MoS₂ sheets in the thinnest film is shown in Figure 1c. The surface morphology of the perovskite thin films deposited using a simple one-step spin-coating method is shown in Figure 1d. The fibril-like network morphology of the perovskite is consistent with the structure reported previously by

other groups employing similar deposition method.^[21,22] Planar structure perovskite photodetectors employing this method provide advantages of uniformity, photosensitivity and flexibility.

To investigate the optical properties of the hybrid MoS₂/CH₃NH₃PbI₃ films, UV-vis and steady-state photoluminescence (PL) spectroscopy measurements were conducted. UV-vis absorption results of pristine MoS₂ films (1T and 2H phases) and pristine CH₃NH₃PbI₃ film are presented in Figure 1e. As deposited pristine MoS₂ nanosheet films exhibit no obvious absorption peaks due to their high 1T phase concentration, rendering them metallic. In contrast, annealed MoS₂ films that are semiconducting 2H phase show typical peaks that can be attributed to the A and B excitons arising from the K point of the Brillouin zone between 600 and 700 nm.^[23] Absorption of pristine perovskite film show an obvious absorption edge around 760 nm corresponding to its direct optical bandgap.^[24] We also illustrated absorption results of different thickness of pristine MoS₂ films and hybrid MoS₂/ CH₃NH₃PbI₃ film in the supplementary information (Figure S2). After deposition of the perovskite layer, the two absorption peaks of 2H-MoS₂ remain visible. To further confirm the phase of MoS₂, we conducted Raman and XPS spectroscopies on pristine MoS₂ films (Figure S3 and Figure S4). Two prominent peaks corresponding to the in-plane E_{2g}¹ (382 cm⁻¹) and out-of-plane A_{1g} (405 cm⁻¹) modes of 2H-MoS₂ can be seen clearly. Chemically exfoliated samples exhibit weak peaks in the lower frequency region, referred to as J1, J2, and J3, that correspond to modes that are active in 1T-MoS₂.^[25] The two samples of MoS₂ were identified by XPS in Mo 3d, S 2s, and S 2p regions. It has been confirmed that the peaks from the 1T phase appear at a binding energy that is ~0.9 eV lower than the 2H phase.^[26] Figure 1g shows the PL spectra of the CH₃NH₃PbI₃ and MoS₂/CH₃NH₃PbI₃ samples prepared under the same conditions. As we can

see from the figure, both samples exhibited a PL peak at ~ 767 nm arising from the bandgap of perovskite (~ 1.6 eV), which can be attributed to band-to-band recombination.^[27,28] However, a dramatic quenching was observed for both 1T-MoS₂/CH₃NH₃PbI₃ and 2H-MoS₂/CH₃NH₃PbI₃ hybrid films. Specifically, the peak intensity of hybrid 2H-MoS₂/CH₃NH₃PbI₃ was quenched by $\sim 60\%$ with respect to the peak intensity of pure perovskite film, resulting from charge transfer from perovskite to 2H-MoS₂. Moreover, the peak intensity of hybrid 1T-MoS₂/CH₃NH₃PbI₃ was quenched by $\sim 90\%$, indicating more effective charge transfer from perovskite to 1T-MoS₂. In addition, we observed higher quenching for films with continuous coverage and multi-layered MoS₂.

The efficient charge transfer from perovskite to MoS₂ indicated by the PL quenching suggests that the MoS₂/CH₃NH₃PbI₃ heterostructure photodetectors should exhibit good photoresponse. The current-voltage curves of 1T-MoS₂/CH₃NH₃PbI₃ devices under dark and 100 mW/cm² white light illumination with different thicknesses of MoS₂ films are shown in Figure 2a. The typical linear and symmetrical plots of dark current and photocurrent versus voltage indicate that hybrid 1T-MoS₂/CH₃NH₃PbI₃ form low resistance contacts with the gold electrodes. The dark current of the device increases almost three orders with increasing thickness of MoS₂. Owing to the more efficient electron transfer from perovskite to thicker MoS₂, the resulting photocurrent ($I_{ph} = I_{illuminated} - I_{dark}$) also surges with increasing thickness of MoS₂ in the photodetector at the same bias voltage. The responsivity and External Quantum Efficiency (EQE) of devices with thinnest MoS₂ films are illustrated in Figure 2b under illumination wavelengths between 400 to 850 nm and bias of 2 V. The responsivity (R) of a photodetector is defined as $\frac{I_{ph}}{P}$, where I_{ph} and P are the photocurrent density (mA/cm²) and

incident illumination power density (mW/cm^2), respectively. The EQE of a photodetector can be calculated by $EQE = R \times E \times 100$, where R and E are the responsivity (A/W) and the incident photon energy (J), respectively. As the wavelength increases, there is an obvious decline for both responsivity and EQE above 770 nm which is attributed to the excitation of charges in the perovskite layer. At a light power density of $37.9 \mu\text{W}/\text{cm}^2$ and wavelength of 500 nm, the 1T phase hybrid photodetector exhibits a responsivity of 3096 A/W and an EQE of $7.7 \times 10^5 \%$, which is comparable to reported CVD processed graphene/perovskite or 2D material ($\text{MoS}_2, \text{WS}_2$)/perovskite hybrid photodetectors.^[9,10,13,14,29] It is worth noting that with multi-layered 1T- MoS_2 film in the hybrid photodetector, we can get even higher responsivity and EQE. However, the on/off ratio of the 1T- $\text{MoS}_2/\text{CH}_3\text{NH}_3\text{PbI}_3$ is limited by the high dark current, as also observed in the case of graphene/ $\text{CH}_3\text{NH}_3\text{PbI}_3$ photodetectors.^[9-11,29,30] This is attributed to the high conductivity of graphene, and in our case metallic 1T- MoS_2 . As seen from Figure 2a, the on/off ratios are all lower than 2, which make such photodetectors impractical for integrated circuit devices, despite their exceptionally high responsivity.

To address the on/off ratio, we investigated devices using 2H phase MoS_2 nanosheets. The current-voltage curves of 2H- $\text{MoS}_2/\text{CH}_3\text{NH}_3\text{PbI}_3$ heterostructure devices under dark and $100 \text{ mW}/\text{cm}^2$ white light illumination with different thickness of MoS_2 films are presented in Figure 2c. Similar to the 1T phase MoS_2 devices, the linear and symmetrical dark current and photocurrent versus voltage show that the contacts are low resistance. The dark current of the device increases with increasing thickness of MoS_2 . More significantly however, the on/off ratio increases significantly relative to the metallic 1T phase MoS_2 devices, reaching a value of ~ 300 . Our results demonstrate that there is a compromise between responsivity and on/off ratio in the performance of the hybrid photodetectors. The responsivity and EQE results of the multi-

layered 2H phase MoS₂ devices are illustrated in Figure 2d under different illumination wavelengths at a bias of 2 V. At a light power intensity of 31.3 μW/cm² at 500 nm wavelength, the multi-layered 2H phase hybrid photodetector exhibits a responsivity of 142 A/W and a EQE of 3.5 × 10⁴ %, which is much better than CVD-deposited monolayer MoS₂ phototransistors^[31] and pure perovskite film photodetectors.^[32–34]

We have also explored photoresponsivity dependence of both hybrid structures on light intensity. The current-voltage curves of 1T-MoS₂/CH₃NH₃PbI₃ and 2H-MoS₂/CH₃NH₃PbI₃ photodetectors under 500 nm illumination at power ranging from 0.14 to 13.27 μW are shown in Figures 3a and 3c, respectively. From these curves, we can see that the photocurrent of both structures rise with the increasing illumination light power. We also observe this rising trend when considering the responsivities at different thickness of MoS₂ as a function of illumination power, as summarized in Figures 3b and 3d for the 1T and 2H phases, respectively. As a result, we can obtain a responsivity of 3.3 × 10⁵ A/W for multi-layered 1T-MoS₂/CH₃NH₃PbI₃ devices at a power of 0.14 μ W, the highest value measured in this study.

Another important parameter of a photodetector is photodetectivity (D*), which is defined as $\frac{(A\Delta f)^{\frac{1}{2}}R}{i_n}$ where A is the working area of the device, Δf is the electrical bandwidth and i_n is the noise current.[13] If, as expected, the shot noise from the dark current is the major contribution, the detectivity can be expressed as $R\left(\frac{A}{2qI_d}\right)^{1/2}$ where q is the absolute value of electron charge (1.6 × 10⁻¹⁹ Coulombs) and I_d is the dark current. The detectivities of multi-layered 1T-MoS₂/CH₃NH₃PbI₃ devices and 2H-MoS₂/CH₃NH₃PbI₃ devices are depicted in Figure 3b and 3d. Owing to the enhanced responsivity, D* was found to exceed 10¹¹ Jones at 0.14 μ W, specifically, 7 × 10¹¹ Jones was measured for the 1T phase multi-layered devices and 2.6 × 10¹¹ Jones for 2H devices. The detectivity we obtained is better than that reported for

heterostructure graphene/perovskite photodetectors. Importantly, we can adjust the phase and thickness of MoS₂ to gain better performance of the detectors by this solution process method. Detailed performance parameters of reported heterostructure perovskite-based photodetectors are listed in Table 1.

Finally, the temporal photoresponse of the 1T-MoS₂/CH₃NH₃PbI₃ and 2H-MoS₂/CH₃NH₃PbI₃ photodetectors was tested under periodic illumination with an on/off interval of 4 s. The on/off switching behavior was preserved over multiple cycles. Current with respect to time is shown in Figure 4a and 4c for 1T and 2H phase devices, respectively. It is revealed that the photocurrents of both hybrid photodetectors are consistent and repeatable. The rise and decay time are defined as when the photocurrent and the dark current increase or decrease by 80% compared to their peak value.^[33] The rise and decay times for the hybrid 1T-MoS₂/CH₃NH₃PbI₃ device were measured to be 0.45 s and 0.75 s. In contrast, the 2H-MoS₂/CH₃NH₃PbI₃ device is faster by one order of magnitude. The rise time is less than 25 ms which is the detection limit of our equipment and the decay time is less than 50 ms, which is much faster than graphene based perovskite photodetectors.^[9,10,29]

In conclusion, we have investigated the opto-electronic properties of solution processed hybrid photodetectors based on chemically exfoliated 2D MoS₂ nanosheets and organolead halide perovskites. We studied the influence of metallic and semiconducting phases of 2D MoS₂ on the performance of hybrid photodetectors. We found that it is possible to achieve exceptionally high photoresponsivity and EQE values for hybrid photodetectors consisting of 1T phase nanosheets integrated with perovskites. However, the metallic nature of the 1T phase leads to high dark currents, which in turn leads to impractical on/off ratios. In contrast, semiconducting 2H phase can mitigate the low on/off ratio while providing photoresponsivity

and detectivity. Our work provides insights into how different phases of 2D materials can be utilized for photodetection to mitigate key challenges.

Experimental Section

Materials: All chemicals, unless stated otherwise, were purchased from Sigma-Aldrich without further purification.

Chemical exfoliation of MoS₂: Chemically exfoliated MoS₂ was synthesized by lithium intercalation into bulk MoS₂ powder as reported previously.^[15] Namely 3 mL of 1.6 M n-butyllithium was added to 0.3 g of bulk MoS₂ powder under argon and refluxed for 48 h. The mixture was then filtered and washed with hexane to remove any excess of butyllithium or other organic residue. The intercalated powder was then exfoliated in water at 1.5 mg/mL, sonicated for 1 h and centrifuged to remove lithium cations as well as the non-exfoliated bulk material.

Perovskite: CH₃NH₃I was synthesized by mixing 24 mL of methylamine with 10 mL of hydroiodic acid in a round-bottom flask at 0 °C for 2 h with stirring. The solvent was removed by heating the solution in a rotary evaporator at 50 °C. The white precipitate of raw CH₃NH₃I was washed by ethanol, filtered and then washed by diethyl ether again. This procedure was repeated three times. After the last filtration, the products were dried at 60 °C in a vacuum oven for 24 h and stored in a glovebox. A 40 wt. % solution of CH₃NH₃PbI₃ was prepared by dissolving PbI₂ and CH₃NH₃I in a 1:1 molar ratio in N, N-dimethylformamide and heating at 70 °C overnight inside an argon filled glovebox.

Device Fabrication: Silicon oxide on silicon substrates were sequentially cleaned in soap water, deionized water, acetone, and ethanol in ultrasonic bath for 15 min, and dried under nitrogen flow. Gold contacts were deposited on top of the substrates using thermal deposition

with a shadow mask. MoS₂ films were prepared using vacuum filtration of chemically exfoliated nanosheets in water using a 25 nm membrane from Millipore, then transferred onto the target substrate. The thickness of the 1T MoS₂ film was varied depending on the volume of the MoS₂ solution filtered. The films can be converted to the 2H phase by annealing the as-exfoliated 1T MoS₂ film in argon at 300 °C for half an hour. The perovskite precursor was spin-coated at 3000 rpm for 60 s on MoS₂ film. The substrates were then heated on a hot plate at 100 °C for 20 min. To improve the device stability in air, layers of PMMA were spin-coated onto the perovskite films at 4000 rpm for 60 s. Finally, the devices were heated on a hot plate at 80 °C for 10 min.

Supporting Information

Supporting Information is available from the Wiley Online Library or from the author.

Acknowledgements

Hang Zhou would like to thank financial support from the Shenzhen Science and Technology Innovation Committee (No.KQCX20140522143114399, JCYJ20160229122349365) .

Received: ((will be filled in by the editorial staff))

Revised: ((will be filled in by the editorial staff))

Published online: ((will be filled in by the editorial staff))

- [1] M. Chhowalla, H. S. Shin, G. Eda, L.-J. Li, K. P. Loh, H. Zhang, *Nat. Chem.* **2013**, *5*, 263.
- [2] R. Lu, C. Christianson, B. Weintrub, J. Z. Wu, *ACS Appl. Mater. Interfaces* **2013**, *5*, 11703.
- [3] G. Konstantatos, M. Badioli, L. Gaudreau, J. Osmond, M. Bernechea, F. P. G. de Arquer, F. Gatti, F. H. L. Koppens, *Nat. Nanotechnol.* **2012**, *7*, 363.
- [4] F. H. L. Koppens, T. Mueller, P. Avouris, A. C. Ferrari, M. S. Vitiello, M. Polini, *Nat. Nanotechnol.* **2014**, *9*, 780.
- [5] M. R. Esmaili-Rad, S. Salahuddin, *Sci. Rep.* **2013**, *3*, DOI 10.1038/srep02345.
- [6] S. H. Yu, Y. Lee, S. K. Jang, J. Kang, J. Jeon, C. Lee, J. Y. Lee, H. Kim, E. Hwang, S. Lee, J. H. Cho, *ACS Nano* **2014**, *8*, 8285.
- [7] S. D. Stranks, G. E. Eperon, G. Grancini, C. Menelaou, M. J. P. Alcocer, T. Leijtens, L. M. Herz, A. Petrozza, H. J. Snaith, *Science* **2013**, *342*, 341.
- [8] W. Nie, H. Tsai, R. Asadpour, J.-C. Blancon, A. J. Neukirch, G. Gupta, J. J. Crochet, M. Chhowalla,

- S. Tretiak, M. A. Alam, H.-L. Wang, A. D. Mohite, *Science* **2015**, *347*, 522.
- [9] Y. Lee, J. Kwon, E. Hwang, C.-H. Ra, W. J. Yoo, J.-H. Ahn, J. H. Park, J. H. Cho, *Adv. Mater.* **2015**, *27*, 41.
- [10] M. Spina, M. Lehmann, B. Náfrádi, L. Bernard, E. Bonvin, R. Gaál, A. Magrez, L. Forró, E. Horváth, *Small* **2015**, *11*, 4824.
- [11] Z. Sun, L. Aigouy, Z. Chen, *Nanoscale* **2016**, *8*, 7377.
- [12] M. He, Y. Chen, H. Liu, J. Wang, X. Fang, Z. Liang, *Chem Commun* **2015**, *51*, 9659.
- [13] D.-H. Kang, S. R. Pae, J. Shim, G. Yoo, J. Jeon, J. W. Leem, J. S. Yu, S. Lee, B. Shin, J.-H. Park, *Adv. Mater.* **2016**.
- [14] C. Ma, Y. Shi, W. Hu, M.-H. Chiu, Z. Liu, A. Bera, F. Li, H. Wang, L.-J. Li, T. Wu, *Adv. Mater.* **2016**, *28*, 3683.
- [15] G. Eda, H. Yamaguchi, D. Voiry, T. Fujita, M. Chen, M. Chhowalla, *Nano Lett.* **2011**, *11*, 5111.
- [16] D. Voiry, M. Salehi, R. Silva, T. Fujita, M. Chen, T. Asefa, V. B. Shenoy, G. Eda, M. Chhowalla, *Nano Lett.* **2013**, *13*, 6222.
- [17] M. Acerce, D. Voiry, M. Chhowalla, *Nat. Nanotechnol.* **2015**, *10*, 313.
- [18] Y. Yao, Z. Lin, Z. Li, X. Song, K.-S. Moon, C. Wong, *J. Mater. Chem.* **2012**, *22*, 13494.
- [19] Q. H. Wang, K. Kalantar-Zadeh, A. Kis, J. N. Coleman, M. S. Strano, *Nat. Nanotechnol.* **2012**, *7*, 699.
- [20] L. Wang, Z. Xu, W. Wang, X. Bai, *J. Am. Chem. Soc.* **2014**, *136*, 6693.
- [21] H. Deng, X. Yang, D. Dong, B. Li, D. Yang, S. Yuan, K. Qiao, Y.-B. Cheng, J. Tang, H. Song, *Nano Lett.* **2015**, *15*, 7963.
- [22] K. C. Kwon, K. Hong, Q. Van Le, S. Y. Lee, J. Choi, K.-B. Kim, S. Y. Kim, H. W. Jang, *Adv. Funct. Mater.* **2016**, *26*, 4213.
- [23] K. Wang, J. Wang, J. Fan, M. Lotya, A. O'Neill, D. Fox, Y. Feng, X. Zhang, B. Jiang, Q. Zhao, H. Zhang, J. N. Coleman, L. Zhang, W. J. Blau, *ACS Nano* **2013**, *7*, 9260.
- [24] S. De Wolf, J. Holovsky, S.-J. Moon, P. Löper, B. Niesen, M. Ledinsky, F.-J. Haug, J.-H. Yum, C. Ballif, *J. Phys. Chem. Lett.* **2014**, *5*, 1035.
- [25] S. Jiménez Sandoval, D. Yang, R. F. Frindt, J. C. Irwin, *Phys. Rev. B* **1991**, *44*, 3955.
- [26] P. Joensen, E. D. Crozier, N. Alberding, R. F. Frindt, *J. Phys. C Solid State Phys.* **1987**, *20*, 4043.
- [27] C. Wehrenfennig, M. Liu, H. J. Snaith, M. B. Johnston, L. M. Herz, *J. Phys. Chem. Lett.* **2014**, *5*, 1300.
- [28] F. Deschler, M. Price, S. Pathak, L. E. Klintberg, D.-D. Jarausch, R. Higler, S. Hüttner, T. Leijtens, S. D. Stranks, H. J. Snaith, M. Atatüre, R. T. Phillips, R. H. Friend, *J. Phys. Chem. Lett.* **2014**, *5*, 1421.
- [29] Y. Wang, Y. Zhang, Y. Lu, W. Xu, H. Mu, C. Chen, H. Qiao, J. Song, S. Li, B. Sun, Y.-B. Cheng, Q. Bao, *Adv. Opt. Mater.* **2015**, *3*, 1389.
- [30] V. Q. Dang, G.-S. Han, T. Q. Trung, L. T. Duy, Y.-U. Jin, B.-U. Hwang, H.-S. Jung, N.-E. Lee, *Carbon* **2016**, *105*, 353.
- [31] Y. Z. L. H, L. H, J. L, S. Y, S. Y, L. G, Z. Q, C. X, Z. H, *ACS Nano* **2012**, *6*, 74.
- [32] Y. Zhang, J. Du, X. Wu, G. Zhang, Y. Chu, D. Liu, Y. Zhao, Z. Liang, J. Huang, *ACS Appl. Mater. Interfaces* **2015**, *7*, 21634.
- [33] W. Wang, H. Xu, J. Cai, J. Zhu, C. Ni, F. Hong, Z. Fang, F. Xu, S. Cui, R. Xu, L. Wang, F. Xu, J. Huang, *Opt. Express* **2016**, *24*, 8411.
- [34] Y. Guo, C. Liu, H. Tanaka, E. Nakamura, *J. Phys. Chem. Lett.* **2015**, *6*, 535.
- [35] S. Chen, C. Teng, M. Zhang, Y. Li, D. Xie, G. Shi, *Adv. Mater.* **2016**.
- [36] H.-R. Xia, J. Li, W.-T. Sun, L.-M. Peng, *Chem Commun* **2014**, *50*, 13695.
- [37] Z. Sun, Z. Liu, J. Li, G. Tai, S.-P. Lau, F. Yan, *Adv. Mater.* **2012**, *24*, 5878.

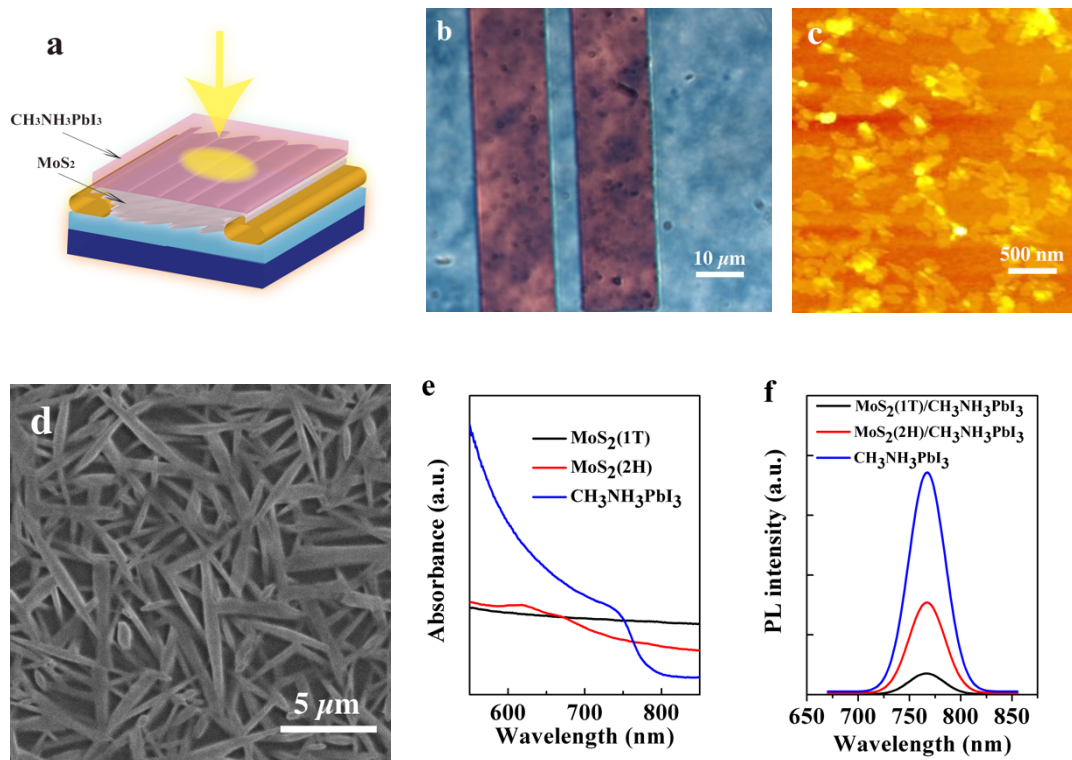
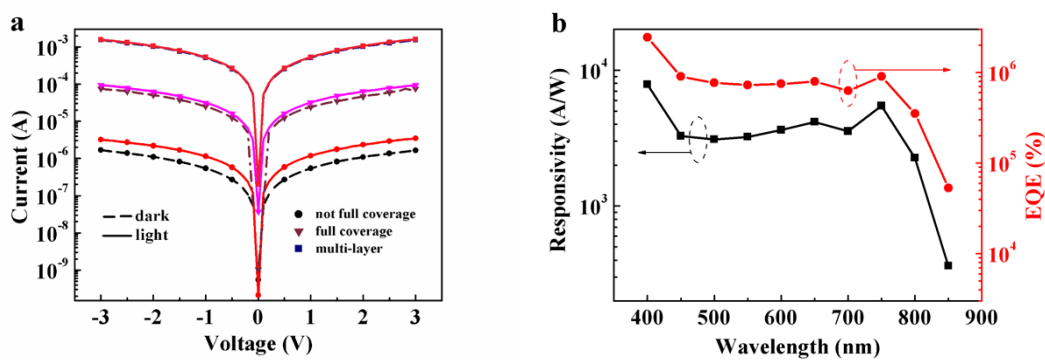


Figure 1. a) Schematic of the photodetection device. b) Optical microscopy image of the multi-layered MoS₂ film on electrodes deposited silicon dioxide showing the MoS₂ channel (blue regions) and gold electrodes (pink regions). c) AFM image of MoS₂ sheets in the thinnest film showing a percolating but not continuous film. d) Typical SEM image of perovskite films on MoS₂ nanosheets. e) UV-vis absorption spectra of pristine MoS₂ and CH₃NH₃PbI₃ films. f) PL spectra of pristine CH₃NH₃PbI₃ and hybrid MoS₂/CH₃NH₃PbI₃ thin films upon excitation at 532 nm.



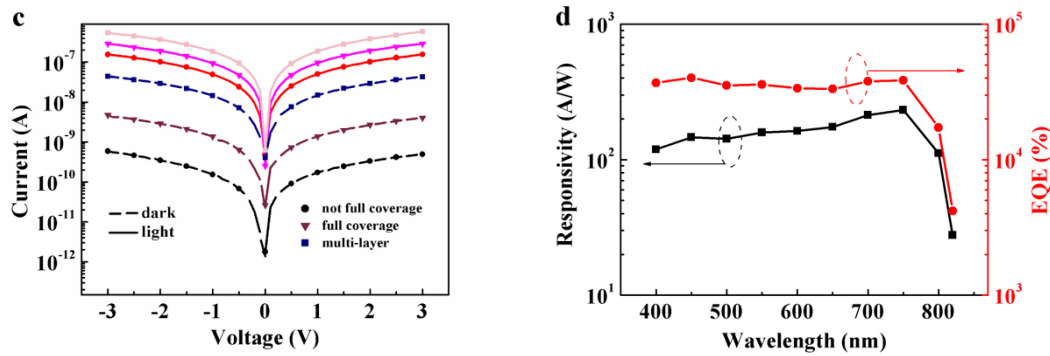


Figure 2. a) I-V curves of 1T-MoS₂/CH₃NH₃PbI₃ in dark and white light with different thickness of MoS₂. b) Responsivity and EQE results of 1T-MoS₂/CH₃NH₃PbI₃ photodetector. The results are for the thinnest 1T phase MoS₂ films. c) I-V curves of 2H-MoS₂/CH₃NH₃PbI₃ in dark and white light with different thickness of MoS₂. d) Responsivity and EQE results of multi-layered 2H-MoS₂/CH₃NH₃PbI₃ photodetector.

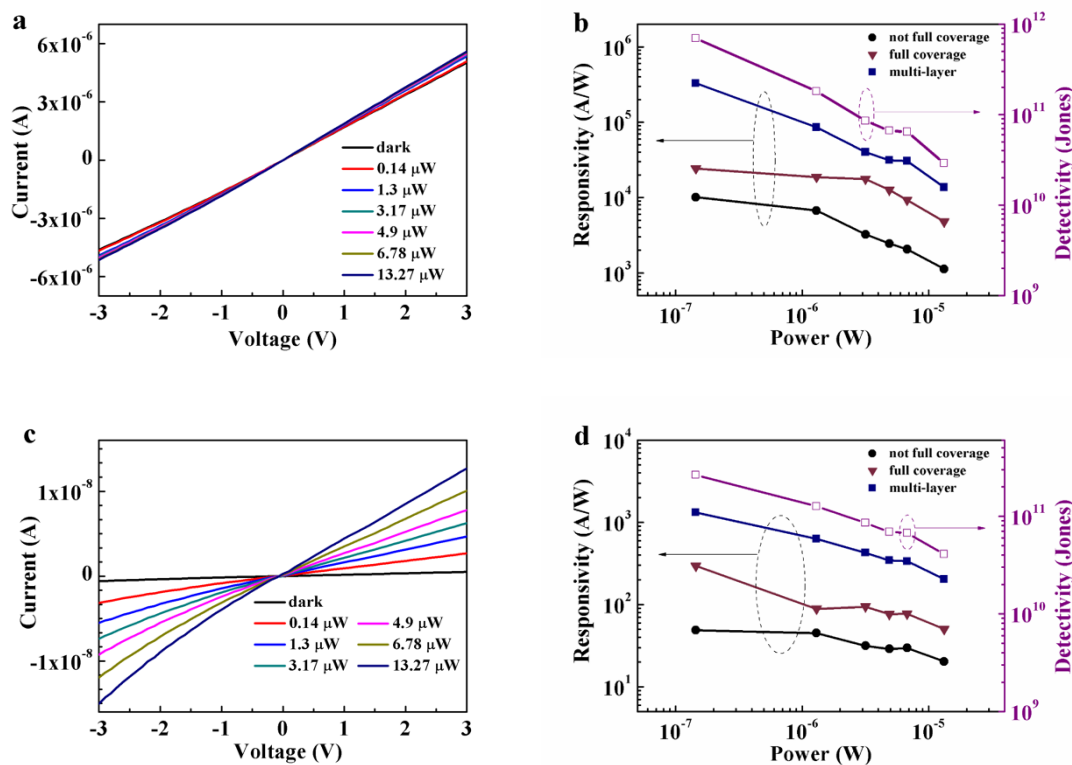


Figure 3. a) I-V plot of the thinnest 1T-MoS₂/CH₃NH₃PbI₃ under various illumination powers. c) I-V plot of the thinnest 2H-MoS₂/CH₃NH₃PbI₃ under powers. b) Responsivities of the 1T-MoS₂/CH₃NH₃PbI₃ photodetectors as a function of various illumination powers. d) Responsivities of the 2H-MoS₂/CH₃NH₃PbI₃ photodetectors as a function of various illumination powers.

Table 1. Performance summary of reported heterostructure perovskite-based photodetectors.

Device structure	Incidence	Responsivity (A/W)	ON/OFF	Rise/fall	Detectivity(J)
------------------	-----------	--------------------	--------	-----------	----------------

MoS ₂ /MAPbI ₃ ^[13]	4.63pW @520 nm	2.12×10^4 @V _g =20 V	~10	10.7 s, 6.2 s	1.38×10^{10}
MAPbI ₃ /PDPP3T ^[35]	0.5 mW/cm ² @365 nm	10.7×10^{-3}		-	6.1×10^9
WS ₂ /MAPbI ₃ ^[14]	0.5 mW/cm ² @505 nm	17	1×10^5	2.7 ms, 7.5 ms	2×10^{12}
Graphene/MAPbI ₃ ^[11]	0.014 mW/cm ² @532 nm	223.5	<2	1.5 s	-
Graphene/MAPbI ₃ ^[30]	0.003 mW	115	<2	5.3 s	3×10^{12}
Graphene/MAPbI ₃ ^[10]	3.3 pW	2.6×10^6		55 s, 75 s	
Graphene/MAPbI ₃ ^[9]	1 uW	180	<2	540 ms	1×10^9
Graphene/MAPbBr ₂ ^[29]	1.052 nW	6×10^5	<2	750 ms	
TiO ₂ /MAPbI ₃ ^[36]	100 mW/cm ²	0.49×10^{-6}	70	0.02 s	

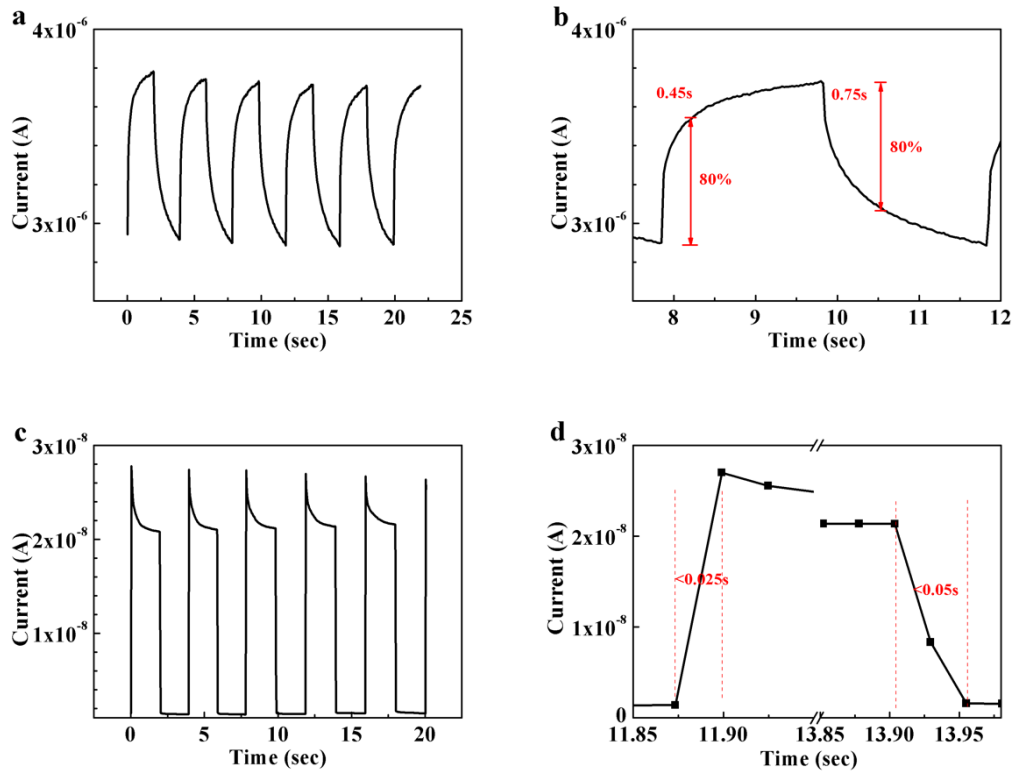


Figure 4. a) Photo-switching characteristics of the 1T-MoS₂/CH₃NH₃PbI₃ photodetector. b) Temporal voltage response of the 1T-MoS₂/CH₃NH₃PbI₃ photodetector, highlighting a rise time of 0.45 s and a decay time of 0.75 s. c) Photo-switching characteristics of the 2H-MoS₂/CH₃NH₃PbI₃ photodetector. d) Temporal voltage response of the 2H-MoS₂/CH₃NH₃PbI₃ photodetector, highlighting a rise time of 0.025 s and a decay time of 0.05 s.

Supporting Information

Solution-processed MoS₂/ organolead trihalide perovskite photodetectors

Yan Wang, Raymond Fullon, Muharrem Acerce, Christopher E. Petoukhoff, Jieun Yang, Chenggan Chen, Songnan Du, Sin Ki Lai, Shu Ping Lau, Damien Voiry, Gautam Gupta, Aditya D. Mohite, Shengdong Zhang, Hang Zhou, and Manish Chhowalla**

S1. Optical microscopy images

The thicknesses of MoS₂ nanosheet films are controlled by solution volume used to deposit the films. Optical images of not fully continuous layer (~80% coverage of the channel surface) and completely continuous channel film with full coverage are given in Figure S1. The blue region is MoS₂ film and the pink region is patterned gold electrode.

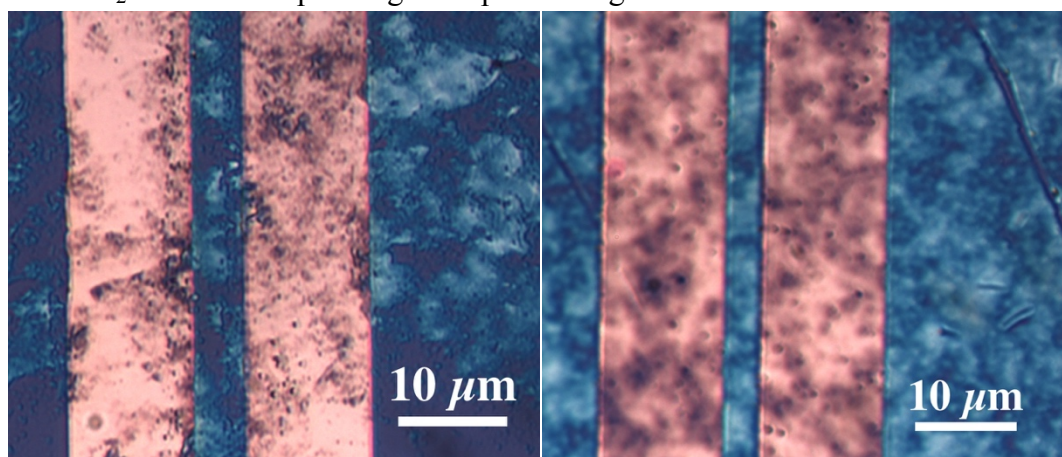


Figure S1. Optical microscopy image of the MoS₂ films on gold patterned silicon oxide.

S2. UV-vis absorption

UV-vis absorption of 2H-MoS₂ and 2H-MoS₂/perovskite layers with different MoS₂ thicknesses are given in Figure S2. 2H-MoS₂ films show typical peaks that can be attributed to the A and B excitons arising from the K point of the Brillouin zone between 600 and 700 nm. After depositing perovskite layer, the two absorption peaks of 2H-MoS₂ remain visible, as labeled in the figure. In addition, typical absorption edge around 760 nm is also obvious in the hybrid structure.

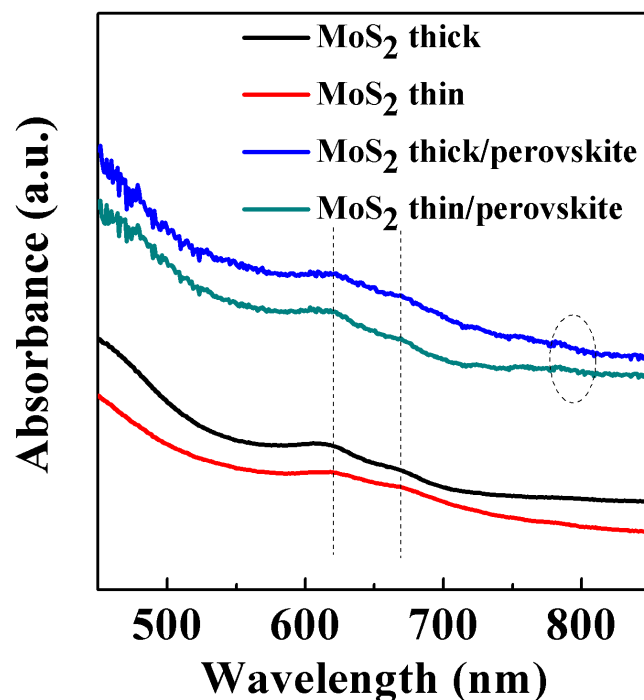


Figure S2. Absorption of MoS₂ films and MoS₂/perovskite layers.

S3. Raman spectroscopy

Raman spectra of chemically exfoliated 1T-MoS₂ film and annealed 2H-MoS₂ film are given in Figure S3. Two prominent peaks corresponding to the in-plane E_{2g}¹ (382 cm⁻¹) and out-of-plane A_{1g} (405 cm⁻¹) modes of 2H-MoS₂ can be seen clearly. Chemically exfoliated samples exhibit weak peaks in the lower frequency region, referred to as J1, J2, and J3, correspond to modes that are active in 1T-MoS₂.

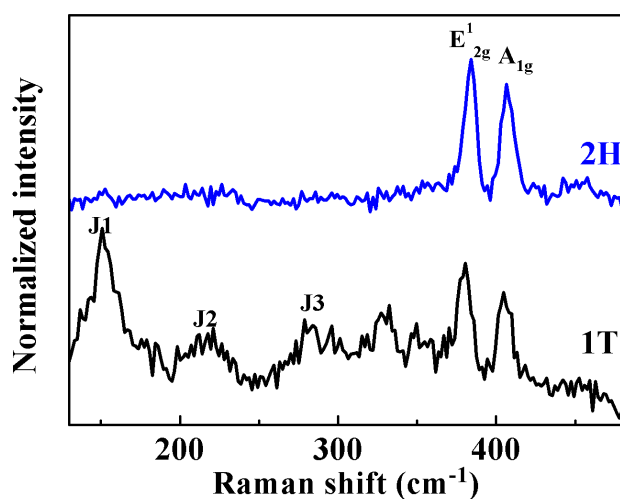


Figure S3. Raman spectra of chemically exfoliated 1T-MoS₂ film and annealed 2H-MoS₂ film.

S4. XPS

X-ray photoemission spectroscopy (XPS) measurements for the binding energies of Mo and S in the MoS₂ are given in Figure S4. The two samples of MoS₂ were identified by XPS in Mo 3d, S 2s, and S 2p regions. It has been confirmed that the peaks from the 1T phase appear at a binding energy that is ~0.9 eV lower than the 2H phase.

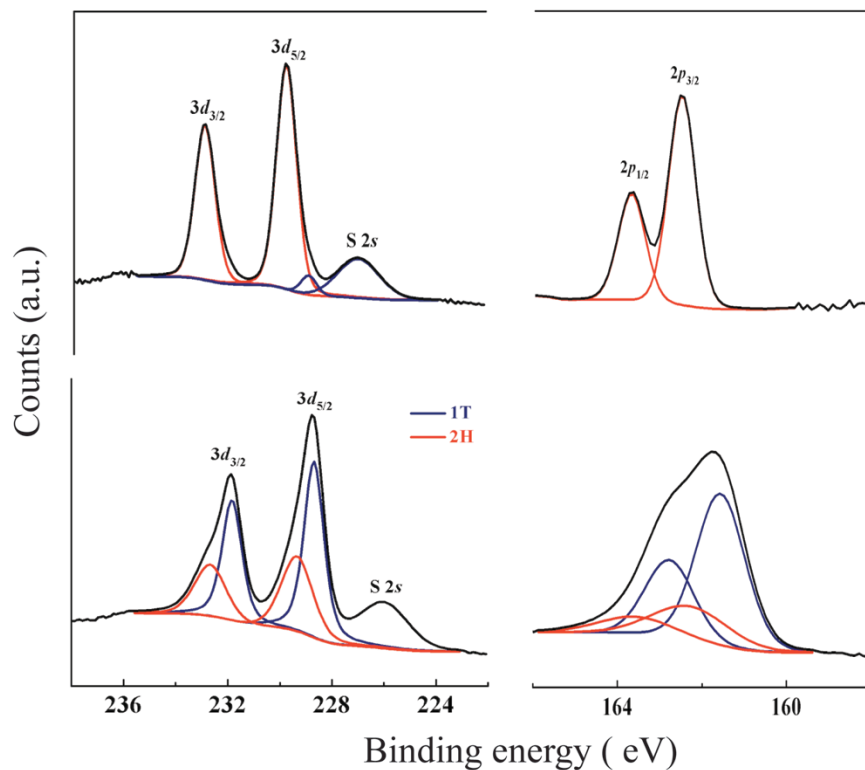


Figure S4. X-ray photoemission spectroscopy (XPS) measurements for the binding energies of Mo and S in two phases of MoS₂.